

## Bluff-body propulsion produced by combined rotary and translational oscillation

H. M. Blackburn<sup>a)</sup>

*CSIRO, Division of Building, Construction and Engineering, Highett, Victoria 3190, Australia  
and Department of Mechanical Engineering, Monash University, Clayton, Victoria 3168, Australia*

J. R. Elston and J. Sheridan

*Department of Mechanical Engineering, Monash University, Clayton, Victoria 3168, Australia*

(Received 27 July 1998; accepted 2 October 1998)

Flows produced by combined oscillatory translation and rotation of a circular cylinder in quiescent fluid have been studied using a two-dimensional direct numerical simulation technique. Results are presented for one set of the five dimensionless groups which characterize these flows, for which it is found that a streaming flow normal to the axis of translation is generated. The consequent reaction force is then used to propel the cylinder in the direction opposite to the jet, thus demonstrating a novel propulsion mechanism for bluff bodies. © 1999 American Institute of Physics.

[S1070-6631(99)02301-6]

In general, bluff-body flows are poorly understood, with our present knowledge being based almost exclusively on experiment, both physical and numerical. Consequently it is still possible for new phenomena to be discovered as new classes of investigation are initiated. The present work deals with a numerical investigation of a new class of bluff-body flows created by combining rectilinear and rotational oscillation of a circular cylinder, the prototypical bluff body.

Two canonical flows associated with an infinitely long circular cylinder are those produced by steady and simple harmonic rectilinear motion of the surrounding fluid past the cylinder. For steady flow of fluid, velocity  $U$ , past a cylinder, diameter  $D$ , the resulting wake can be uniquely characterized by a single dimensionless parameter, the Reynolds number  $Re = UD/\nu$ . The flow that results for all but the lowest Reynolds numbers is the well-known Kármán vortex street, which has an associated vortex shedding frequency  $f_v$ , dimensionlessly quantified as the Strouhal number  $St = f_v D/U$ , and a wake that possesses an alternating asymmetry about its centerline. For the second case of simple harmonic rectilinear motion of the surrounding fluid (or, equivalently, simple harmonic translation of the cylinder in a body of quiescent fluid), two dimensionless groups are required to characterize the flows, typically the Keulegan–Carpenter number  $KC = U/f_t D = 2\pi A_t/D$  and the Reynolds number  $Re = UD/\nu$ , where  $U$  now is the peak translational velocity and  $f_t$ ,  $A_t$  are, respectively, the frequency and amplitude of simple harmonic motion. For moderately low  $KC$  values, oscillating a cylinder in quiescent fluid results in a streaming flow along the translation axis, with reflectional symmetry about this line.<sup>1</sup> At higher  $KC$ , a variety of two-dimensional symmetry-breaking bifurcations are observed in the resulting flow patterns.<sup>1,2</sup>

In the case of steady flow past a circular cylinder, the Kármán street wake can be greatly influenced by imposed oscillatory motion of the cylinder, either rectilinear or rotational. In addition to  $Re$ , dimensionless groups describing the

motion amplitude (such as  $KC$  in the case of translational oscillation) and the ratio of imposed motion frequency to the fixed cylinder vortex shedding frequency,  $f_t/f_v$ , are also required to characterize the flow. The greatest interactions between imposed cylinder motion and the wake flow occur at oscillation frequencies close to the Strouhal frequency, when it is found that the shedding frequency can be entrained by the motion frequency. For the case of translational oscillation, the phase relationship between cylinder motion and vortex shedding is observed to vary rapidly with the frequency of imposed motion within the entrainment regime.<sup>3</sup> In addition, a variety of vortex shedding modes have been observed,<sup>4</sup> including classes which break the Kármán street alternating asymmetry. These changes in the wake flows are reflected in variations in the lift and drag forces experienced by the cylinder. In the case of rotational oscillation about the cylinder axis, a substantial effect has been observed on the wake flows, which in turn results in comparatively large effects on lift and drag forces.<sup>5</sup>

These results point to the sensitivity of bluff-body flows to imposed oscillatory motion of the body, both translational and rotational. A class of flows which has not received attention until now is that created by a circular cylinder moving with combined oscillatory translation and rotation in quiescent fluid. If both motions are simple harmonic, the flows are characterized by five dimensionless groups, which correspond to two sets of Reynolds and Keulegan–Carpenter numbers (one set for translational and the other for rotary motion), and the phase angle  $\phi$  between these two motions. We have assigned the imposed translational motion to be in the vertical direction, so that

$$y(t) = A_t \cos(2\pi f_t t), \quad (1)$$

while the rotational motion of the cylinder about its axis is described by

$$\theta(t) = A_\theta \cos(2\pi f_\theta t + \phi), \quad (2)$$

with counterclockwise rotation corresponding to positive  $\theta$ . We have used two-dimensional numerical simulations in order to carry out an exploratory study of the resulting flows for a small subset of the five dimensionless groups.

The numerical technique used for this study employs a spectral element spatial discretization in conjunction with a second-order time integration scheme based on operator splitting and backwards differencing.<sup>6,7</sup> To provide for cylinder translational motion, but with low computational overhead, the incompressible Navier–Stokes equations are solved in an accelerating reference frame attached to the cylinder, so that the mesh does not deform with time, but the boundary conditions and distributed forcing are continually adjusted during the simulation. The technique has previously been described and applied to simulations of both flows past oscillating cylinders and vortex-induced vibration.<sup>8</sup> The same method has been used in the present work with little modification except as required to introduce tangential rotational motion at the cylinder surface. The method uses a velocity–pressure formulation, and vorticity (used in presentation of results below) was computed in postprocessing via collocation differentiation. Tracking of fluid particles was accomplished using a third-order-in-time predictor–corrector scheme.

In checks carried out with the cylinder oscillating with translational motion in quiescent fluid,  $KC = \pi$ , it was found that the peak forces exerted on the cylinder were converged to four significant figures when eight-order tensor-product Gauss–Lobatto–Legendre polynomial shape functions were used in each element. Temporal convergence checks showed the peak forces to be the same to four-figure accuracy for both  $\Delta t U/D = 0.005$  and  $\Delta t U/D = 0.0025$ . For the results presented here, tenth-order polynomials and  $\Delta t U/D = 0.0025$  were used.

For our study, the Keulegan–Carpenter and Reynolds numbers for the translational motion were held fixed at values of  $\pi$  and  $200 \times 2^{1/2}$ , respectively. The frequency of the rotational oscillation was the same as for the translational oscillation, i.e.,  $f_t = f_\theta$ , while the amplitude of the rotational motion was set so as to make the peak tangential speed on the surface of the cylinder the same as the peak translational speed, i.e.,  $A_\theta = 1$  rad. These choices fix four of the five dimensionless groups. The remaining group, the phase angle  $\phi$  between the two motions, was then changed in steps of  $\pi/8$  between simulations. The full set of these results will be reported elsewhere, but here we concentrate and expand on the case where the rotational and translational motions are out of phase, i.e.,  $\phi = \pi$ .

Vorticity contours for the resulting flow are illustrated in Fig. 1(a). Contours of positive (counterclockwise) vorticity are shown in black, with negative values shown in gray. Contours are drawn only up to an arbitrary maximum magnitude, so that the regions of most intense vorticity adjacent to the cylinder are left unmarked. Only a small subset of the 144-element,  $20D \times 20D$  biperiodic computational domain is shown, and the time is chosen such that the cylinder is at the maximum point in its vertical motion cycle. Sufficient simulation time (50 motion periods) has elapsed for the flow to approach an asymptotic state.

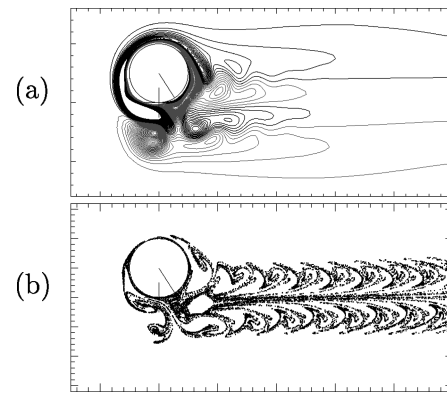


FIG. 1. Flow produced by cylinder with combined oscillatory translation and rotation: (a) instantaneous vorticity contours; (b) fluid particle transport. The cylinder is at its maximum vertical position and most negative angular displacement at the instant shown. The rest position of the cylinder is indicated by cross-hairs, and the radial line shows the rotational displacement of the cylinder.

It is immediately apparent that while the cylinder translation axis is vertical, vorticity transport is predominantly in the horizontal direction. This transport is associated with fluid motion, as illustrated in Fig. 1(b), where the positions of fluid particles released near the cylinder surface are shown. In Fig. 2, a time-mean velocity profile for the  $x$  component of the velocity at a location  $2D$  to the right of the translation axis illustrates the double-peaked nature of the jet flow suggested by the particle transport map. Here the fluid velocity is normalized using the peak translational velocity  $U$ .

The streaming flow normal to the axis of imposed cylinder translation produces an associated time-mean leftwards reaction force on the cylinder. This makes it possible for the cylinder to be propelled in the horizontal direction, something that is comparatively simple to arrange in a computational setting by coupling an ordinary differential equation for the cylinder motion in the horizontal direction (i.e.,  $F_x = ma_x$ ) to the Navier–Stokes equations, as described in previous work.<sup>8</sup> With this done, it was found that the cylinder accelerated to the left (with fluctuations stemming from the comparatively large alternating components of horizontal force), eventually reaching an average terminal speed of 33% of the peak vertical translational speed of the cylinder. Figure 3 illustrates vorticity contours and particle transport for the cylinder “swimming” at terminal speed. Figure 4 shows the time-mean  $x$ -component velocity profile (in a frame of

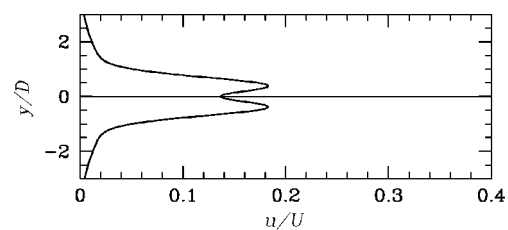


FIG. 2. Mean  $x$ -component velocity profile at  $x/D = 2.0$  for the flow in Fig. 1.

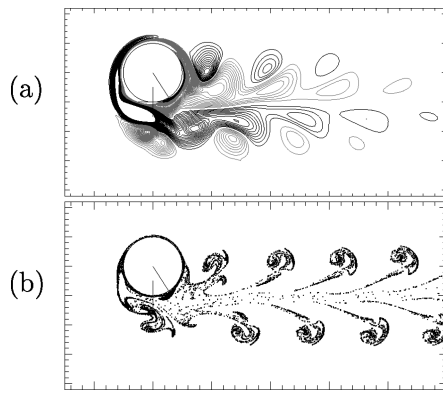


FIG. 3. Propelled cylinder swimming at terminal speed in the  $x$  direction: (a) instantaneous vorticity contours; (b) fluid particle transport.

reference traveling to the left with the cylinder, but fixed in the vertical direction) at  $x/D=2$ .

The mechanism by which the cylinder produces thrust is the subject of continuing investigation. Studying Fig. 1(a) it is clear that the majority of vorticity production occurs on the left face of the cylinder, consistent with the fact that the surface-tangential component of cylinder acceleration is always larger in magnitude on that face.<sup>9</sup> At the instant shown, fluid that has acquired upwards and clockwise momentum on the left-upper face of the cylinder during the motion half-cycle just concluded streams to the right around the upper surface of the cylinder, while below and to the left of the cylinder a detached vortex with counterclockwise rotation has formed. The high-speed rightwards pulsatile flow that occurs above and below the cylinder in each half-motion cycle is reflected in the particle-transport map of Fig. 1(b) and the velocity profile of Fig. 2. With the swimming cylinder, this pulsatile motion is very clearly reflected in the ‘‘puff’’ structures shown in Fig. 3(b).

It is interesting to compare the cylinder motion described here to the carangiform motion employed in fish and bird propulsion.<sup>10</sup> Carangiform motion also consists of a combined phase-locked translation and rotation, but for a rightwards-moving jet flow those motions are typically in

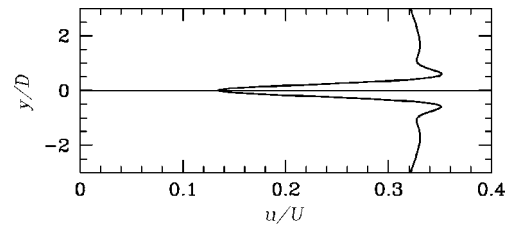


FIG. 4. Mean  $x$ -component velocity profile at  $x/D=2.0$  for the flow in Fig. 3.

phase with one another, while for the bluff-body motion we have described, the translation and rotation are out of phase. This may be linked to the position of the features which act most strongly to influence and control the resulting flows. For flapping foils, it is the Kutta condition at the trailing edge which has the controlling influence, while for the swimming cylinder it would appear instead that the motion of the leading edge is most important.

<sup>a</sup>Electronic mail: Hugh.Blackburn@dbce.csiro.au

<sup>1</sup>M. Tatsuno and P. W. Bearman, ‘‘A visual study of the flow around an oscillating circular cylinder at low Keulegan–Carpenter numbers and low Stokes numbers,’’ *J. Fluid Mech.* **211**, 157 (1990).

<sup>2</sup>C. H. K. Williamson, ‘‘Sinusoidal flow relative to circular cylinders,’’ *J. Fluid Mech.* **155**, 141 (1985).

<sup>3</sup>A. Ongoren and D. Rockwell, ‘‘Flow structure from an oscillating cylinder. 1,’’ *J. Fluid Mech.* **191**, 197 (1988).

<sup>4</sup>C. H. K. Williamson and A. Roshko, ‘‘Vortex formation in the wake of an oscillating cylinder,’’ *J. Fluids Struct.* **2**, 355 (1988).

<sup>5</sup>P. T. Tokumaru and P. E. Dimotakis, ‘‘Rotary oscillation control of a cylinder wake,’’ *J. Fluid Mech.* **224**, 77 (1991).

<sup>6</sup>G. E. Karniadakis, M. Israeli, and S. A. Orszag, ‘‘High-order splitting methods for the incompressible Navier–Stokes equations,’’ *J. Comput. Phys.* **97**, 414 (1991).

<sup>7</sup>R. D. Henderson and G. E. Karniadakis, ‘‘Unstructured spectral element methods for simulation of turbulent flows,’’ *J. Comput. Phys.* **122**, 191 (1995).

<sup>8</sup>H. M. Blackburn and R. D. Henderson, ‘‘Lock-in behaviour in simulated vortex-induced vibration,’’ *Exp. Therm. Fluid Sci.* **12**, 184 (1996).

<sup>9</sup>B. R. Morton, ‘‘The generation and decay of vorticity,’’ *Geophys. Astrophys. Fluid Dyn.* **28**, 277 (1984).

<sup>10</sup>M. J. Lighthill, ‘‘Hydrodynamics of aquatic animal propulsion,’’ *Annu. Rev. Fluid Mech.* **1**, 413 (1969).